Journal of Materials Chemistry A

ROYAL SOCIETY OF CHEMISTRY

COMMUNICATION

View Article Online
View Journal | View Issue

Cite this: J. Mater. Chem. A, 2020, 8, 2343

Received 13th November 2019
Accepted 31st December 2019

DOI: 10.1039/c9ta12489f

rsc.li/materials-a

Dynamical evolution of the 2D/3D interface: a hidden driver behind perovskite solar cell instability†

Albertus A. Sutanto, [a] Nikita Drigo,[a] Valentin I. E. Queloz, [a] Inés Garcia-Benito,[a] Ahmad R. Kirmani, [‡b] Lee J. Richter, [b] Pascal A. Schouwink,[c] Kyung Taek Cho, [a] Sanghyun Paek, [a] Mohammad Khaja Nazeeruddin [*a] and Giulia Grancini [*ad]

Engineering two-/three-dimensional (2D/3D) perovskite solar cells is nowadays a popular strategy for efficient and stable devices. However, the exact function of the 2D/3D interface in controlling the long-term device behavior is still obscure. Here, we reveal a dynamical structural mutation of the 2D/3D interface: the small cations in the 3D cage move towards the 2D layer, which acts as an ion scavenger. If structurally stable, the 2D layer physically blocks the ion movement at the interface boosting the device stability. Otherwise, the 2D layer embeds them, dynamically self-transforming into a quasi-2D structure. The judicious choice of the 2D constituent is decisive in controlling the 2D/3D kinetics and improving the device lifetime, opening a new avenue for perovskite interface design.

Introduction

Within the last decade, perovskite solar cells (PSCs) have been receiving great attention in the area of new generation photovoltaics, with power conversion efficiency (PCE) recently surpassing 25%.[1] Careful interface engineering between the perovskite active layer (AL) and the device interface, *i.e.* the electron or hole transporting layer (ETL/HTL), is the key to device development and optimization. Various engineering strategies have been explored, including interface functionalization with bulky organic molecules,[2] inert polymeric layers,[3–5] inorganic interlayers,[6,7] and graphene or parent 2D materials.[8–10] Alternatively, layered perovskites, popularly referred to as 2D perovskites,[11,12] have been incorporated into the AL-ETL or -HTL interface, forming graded 2D/3D interfaces.[13–18] Thanks to the superior robustness of the 2D perovskite compared to the parent 3D perovskite, such 2D/3D architectures have attracted growing interest as a route to stable and efficient devices.[2] For instance, a combination of methylammonium (MA) lead iodide perovskite and aminovaleric acid-based 2D perovskite resulted in solar cells with greater than 1 year stability, demonstrating the robust nature of combined systems.[19] The 2D perovskite has been shown to simultaneously function as a protective layer and surface defect passivant.[17,20,21] However, whether the 2D perovskite is an essential ingredient for future PSC technology or a popular transitory trend is an open question.[22,23] To answer this point, it is imperative to understand how the 2D perovskite affects the quality of the 3D perovskite surface, and the processes therein, as well as the ultimate device behavior, performance and stability over time.

Here, we report the observation of a slow evolution of the performance of 2D/3D PSCs using a new family of thiophene alkylammonium-based organic cations as building blocks for the layered 2D perovskites and its impact on the device efficiency and stability. We reveal a double effect: first, unexpectedly, during aging for several months in a dark and dry environment, the PSC efficiency increases (from 15% to over 20% in the most striking case), mainly associated with an enhancement of the device open circuit voltage (V_{oc}). While this is found to be true also for the control device, a significant boost is observed as derived from a slow structural rearrangement of the 2D/3D interface. We attribute this to the "soft" nature of the 2D perovskite overlayer that can act as an ion-scavenger. As a consequence of ion movement from the 3D layer towards the interface, small MA cations accumulate at the interface. As a getter, the 2D structure can incorporate the MA cations by self-modifying its pure layered structure into a quasi-2D (or mixed)

[a]Group for Molecular Engineering of Functional Materials, Institute of Chemical Sciences and Engineering, École Polytechnique Fédérale de Lausanne (EPFL), Valais Wallis, Rue de l'Industrie 17, CH-1951 Sion, Switzerland. E-mail: mdkhaja.nazeeruddin@epfl.ch

[b]Materials Science and Engineering Division, National Institute of Standards and Technology (NIST), Gaithersburg, MD, 20899, USA

[c]Institut des Sciences et Ingénierie Chimiques, École Polytechnique Fédérale de Lausanne, Valais Wallis, CH-1951 Sion, Switzerland

[d]Dipartimento Di Chimica, University of Pavia, Via T. Taramelli 14, 27100 Pavia, Italy. E-mail: giulia.grancini@unipv.it

† Electronic supplementary information (ESI) available. See DOI: 10.1039/c9ta12489f

‡ Guest Researcher @Materials Science and Engineering Division, National Institute of Standards and Technology (NIST), Gaithersburg, MD, 20899, USA.

phase.[11] This interface modification generally improves the device performance. On the other hand, depending on the chemical nature of the 2D perovskite, a "more robust" 2D layer can prevent such structural change, physically blocking the ion movement. This leads to a dramatic increase in the device stability, retaining 90% of the initial value under continuous illumination over 1000 hours. The structural change with time has been monitored over a time window of months combining solar cell operation with thin film structural and optical characterization on aged samples and/or under different aging conditions (*i.e.* different thermal stress). Overall, results reveal that the conscious choice of proper 2D components can control the dynamical evolution of the 2D/3D interface and is a key element to control for the realization of efficient and stable devices.

Results and discussion

We synthesized a series of bulky thiophene-terminated cations as building blocks for the layered 2D perovskite structure. Chemical formulae of the thiophenealkylammonium salts namely 2-thiophenemethylammonium iodide (2-TMAI), 3-thiophenemethylammonium iodide (3-TMAI), and 2-thiopheneethylammonium iodide (2-TEAI) along with the derived 2D structure are shown in Fig. 1a. Notably, they only differ in the position and length of the alkyl chain connecting the thiophene core and the ammonium entity. The salts were prepared from the commercially available amines and HI (see ESI† for details).

To create the 2D/3D thin films and devices, we dissolved the salts in isopropanol (IPA) and dynamically spin-coated them on top of a triple-cation $[(FAPbI_3)_{0.87}(MAPbBr_3)_{0.13}]_{0.92}(CsPbI_3)_{0.08}$ based 3D perovskite film, where FA stands for formamidinium (see ESI† for details). As a result, a thin layer of 2D perovskite is formed on top of the 3D bulk, as verified by low angle grazing incidence X-ray Diffraction (XRD). Patterns are shown in Fig. 1b. We note the presence of the peaks at 14°, and at 6° and 4° which correspond to (001) diffraction signals from the 3D perovskite, and, at lower angles, from (002) of the layered 2D perovskite, respectively (the 2D crystal structure is either centro-symmetric or near centro-symmetric such that the (001) diffraction, 1 odd, is forbidden or weak). More in detail, the peak at 6° is related to the formation of a pure 2D perovskite, which takes the formula of $R_2(MA)_{n-1}PbI_{3n+1}$ for $n = 1$ (where n defines the number of inorganic layers), while the peak at 4° is related to a mixed phase (or the quasi-2D perovskite) where, in this case, $n = 2$. Depending on the organic salts, slightly different 2D perovskites are formed: for 2-TMAI mostly $n = 2$; for 3-TMAI only $n = 2$; and for 2-TEAI mostly $n = 1$ 2D phase (see also XRD patterns of the pure 2D perovskite in Fig. S1 and S2†). The 2D perovskite layer, ≈50 nm thick, covers the entire 3D surface, as shown in Fig. 1c by top view and cross-sectional scanning electron microscopy (SEM) images. From the top surface image, we could observe that the 2D overlayer smooths out the surface, rendering it less defined in terms of grain boundaries and crystal borders with respect to the 3D surface (Fig. S3†).

We implement these films as AL in standard (n–i–p) device structure solar cells (see ESI†). The optimized thiophenealkylammonium salt concentration implemented in the devices is 0.06 M, resulting in an ≈50 nm thick 2D layer on top of the 3D layer (see Table S1† for details). The photovoltaic (PV) response of the thiophene-based 2D/3D cells is shown in Fig. 2, Table 1 (statistics in Table S2 and Fig. S4†). It is worth remarking that commonly device data shown in the literature do not specify the aging status of the measured device, making the comparison among reported PCEs rather difficult. This also hides important information on the slow dynamic behavior of the device interfaces that can alter the PSC performances.[24] Slow processes such as those related to ionic motion are still not yet fully understood[25–27] but are considered as the common source of aging phenomena. To address this point, here we monitor the evolution of the device PV performances by comparing fresh (measured 1 day after device fabrication) and aged devices over months (stored in a dark and dry air environment with the humidity controlled below 10%).

Fresh device PCEs range from 15% to 19% depending on the 2D/3D system. For the control it reaches peak performances

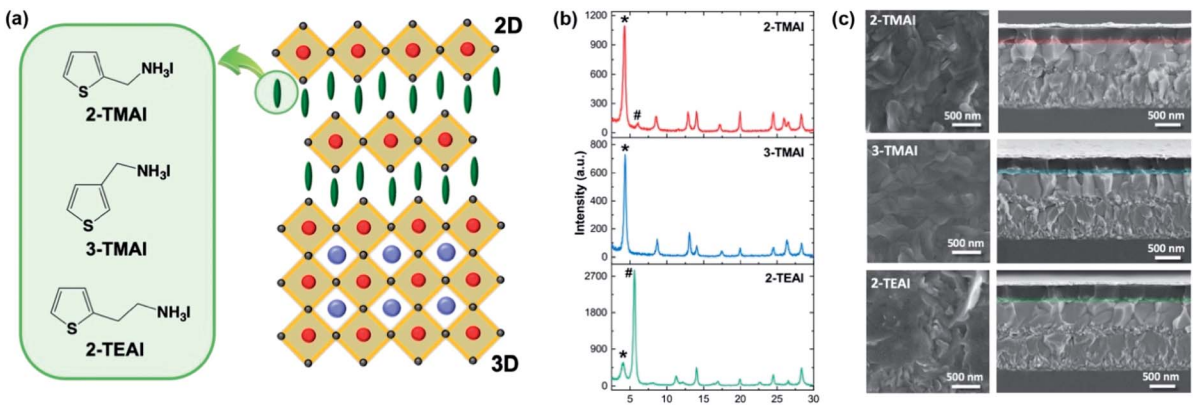

Fig. 1 (a) Molecular structures of the cations (left) and sketch (right) of the derived 2D/3D interface. (b) X-ray diffraction (XRD) pattern at the 2° incident angle of the 2D/3D film employing 2-TMAI, 3-TMAI and 2-TEAI cations in the 2D template. # and * denote diffraction peaks of the 2D perovskite with $n = 1$ and $n = 2$, respectively. (c) Scanning electron microscopy images of the top view (left) of the perovskite films and cross-section (right) of the 2D/3D devices employing 2-TMAI, 3-TMAI and 2-TEAI cations in the 2D layer (highlighted with the colored area).

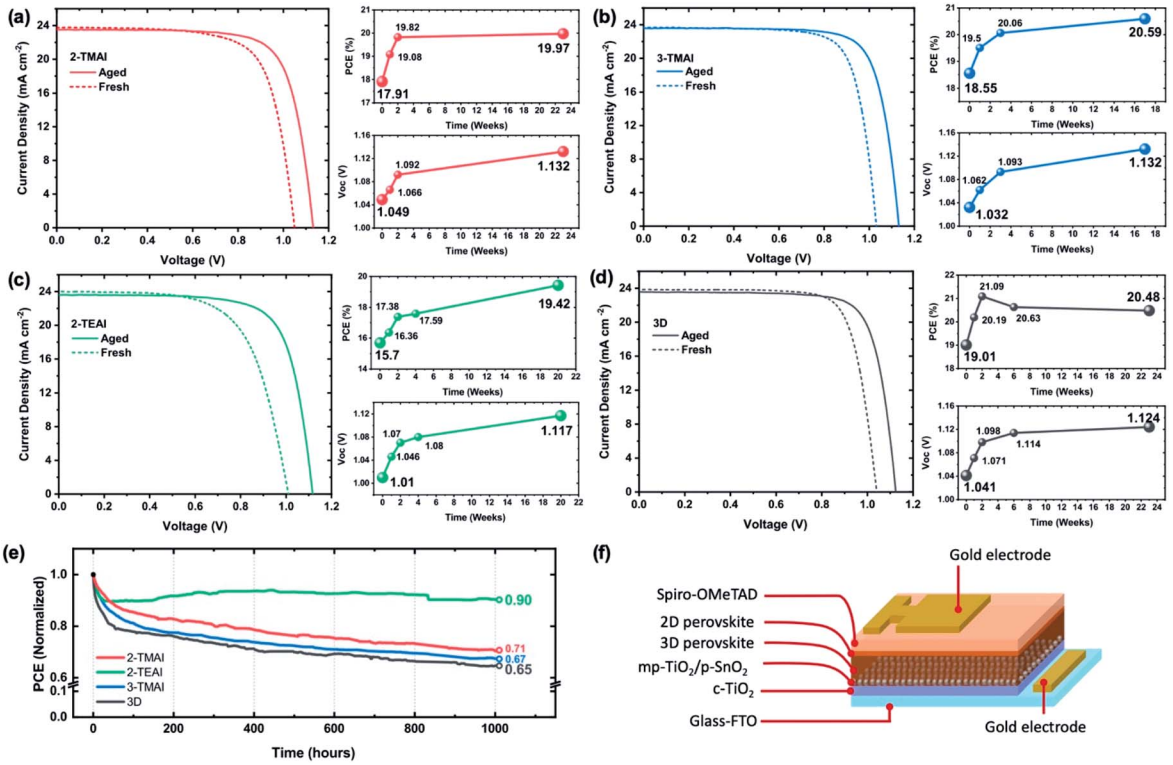

Fig. 2 Photovoltaics characteristics of the 2D/3D PSCs employing (a) 2-TMAI, (b) 3-TMAI and (c) 2-TEAI, (d) 3D control. For each panel the current–voltage characteristics of fresh and aged devices are shown along with the time evolution of the power conversion efficiency (PCE) and open circuit voltage (V_{oc}) of the devices stored in the dark and dry environment (humidity < 10%). (e) Stability test for freshly prepared devices under continuous 1 sun illumination for 1000 h in an Ar atmosphere without any encapsulation. (f) Scheme of the device architecture.

Table 1 Photovoltaic parameters of champion fresh and aged (for a time period as indicated in Fig. 2) 2D/3D PSCs employing 2-TMAI, 3-TMAI, 2-TEAI, and 3D control

Organic cations		V_{oc} (V)	J_{sc} (mA cm^{-2})	FF	PCE (%)
2-TMAI	Fresh	1.049	23.75	0.719	17.91
	Aged	1.132	23.50	0.751	**19.97**
3-TMAI	Fresh	1.032	23.67	0.760	18.55
	Aged	1.132	23.60	0.771	**20.59**
2-TEAI	Fresh	1.010	24.01	0.647	15.70
	Aged	1.117	23.60	0.737	**19.42**
3D	Fresh	1.041	23.87	0.765	19.01
	Aged	1.124	23.57	0.773	**20.48**

after 2 weeks resulting in 21.1% PCE, but decreasing afterwards (Fig. 2d). On the other hand, the 2D/3D systems all show a monotonic improvement in the PCE nearly saturating after 6 months. The aged samples all deliver around 20% PCE with an increase in the device FF and V_{oc}. The 3-TMAI device outperforms the 3D control after aging. Notably, the 2-TEAI 2D/3D systems show the largest improvement of approx. 25% going from 15.70% to 19.42%. Hysteresis and external quantum efficiency (EQE) spectra are reported in Fig. S5 and S6.† This represents our first finding: the presence of the 2D layer improves the performances over time on month-based analysis. Notably, the highest performances of the devices (also the control) are always reached after a few days of storage in the dark and in dry air. However, it is worth mentioning that the final V_{oc} is higher for the 2D/3D system employing 3-TMAI and 2-TMAI. In agreement with previous work on the 2D/3D interface,[28] this can be associated with a surface passivation effect of the 2D layer. To assess that, we investigated the device characteristics under different sunlight intensities, as shown in Fig. S7 and S8† and we find that the 2D layer has a beneficial effect on surface recombination. Studies of the device ideality factor, based on the intensity dependence of the V_{oc} (Fig. S7†) and J_{sc} (Fig. S8†) provide insight into the recombination kinetics in the device.[29,30] Additional interface impedance analysis will be performed to better elucidate the interface recombination channels. Relative to the control, all 2D/3D devices exhibit indeed less monomolecular (trap-mediated) recombination which points toward a reduction of the surface trap density, responsible for the improvement in the V_{oc} and FF. A second important observation relates to device stability where a distinct behavior is observed depending on the nature of the 2D cation. In general, the 2D/3D devices only slightly outperform the 3D reference when measured under continuous 1 sun illumination at the full maximum power point for 1000 h in an inert atmosphere (Fig. 2e) showing, after initial decay as commonly observed for 3D PSCs,[31] a similar degradation curve. Interestingly, the 2-TEAI based 2D/3D device behaves differently: the stability after the initial decay, as commented above, recovers

and is kept at 90% of the initial PCE value with no sign of degradation for the 1000 h tested. This represents a net improvement with respect to the control which decays to 65% of the initial value. To rationalize our finding and elucidate the intimate mechanisms behind such long-term stability, we investigate the evolution with time of the 2D/3D structure by means of photoluminescence (PL) spectral analysis as a simple and immediate method to identify the emissive species, and the related perovskite phase. PL measurements have been carried out over months, mimicking the same time window as for the device tests, as well as fresh but upon different thermal stress, see Fig. 3.

Fig. 3a–c show the PL spectra from the front side (2D perovskite side) of the 2D/3D film exciting both the 2D and the 3D layer for the fresh and aged samples. A weak emission from the 3D perovskite at 770 nm is observed upon front side excitation. Contrarily, upon back side (3D perovskite side) excitation the emission from the 3D perovskite is dominant, see Fig. S9.† For fresh films, peaks at short wavelengths are observed, which appear at: (1) 520 nm and 570 nm for 2-TMAI; (2) 570 nm only for 3-TMAI; (3) 520 nm (dominant) and a shoulder at 550 nm for 2-TEAI. In agreement with XRD analysis, we can assign the 520 nm PL peak to the emission from $n = 1$ 2D perovskite, and the 570 nm peak to $n = 2$ perovskite. This assignment also matches the emission from pure 2D thin films with $n = 1$ or $n = 2$ (see Fig. S10 and S11†). This indicates the formation of distinct 2D perovskite phases depending on the nature of the organic cations. Upon aging, the emission spectra change: (1) 520 nm peak (related to $n = 1$ 2D) vanishes, while the 570 nm peak grows in 2-TMAI; (2) the 570 nm is unchanged, but a new broad peak at a higher wavelength appears in 3-TMAI. This is related to the formation of a mixed 2D film with a higher n value;[11] (3) 2-TEAI based 2D/3D does not show any visible change. This indicates a structural rearrangement of the 2D/3D interface upon aging that holds true for all cases except for the 2-TEAI-2D/3D thin film. A stable $n = 1$ 2D phase upon aging is also observed for PEAI-based 2D/3D systems, confirming the general validity of our observation, see Fig. S12 and S13.† Such structural changes are also confirmed by Grazing Incidence Wide Angle X-ray Scattering (GIWAXS) analysis carried out on aged samples, as shown in Fig. S14.† This observation reveals a structural transformation

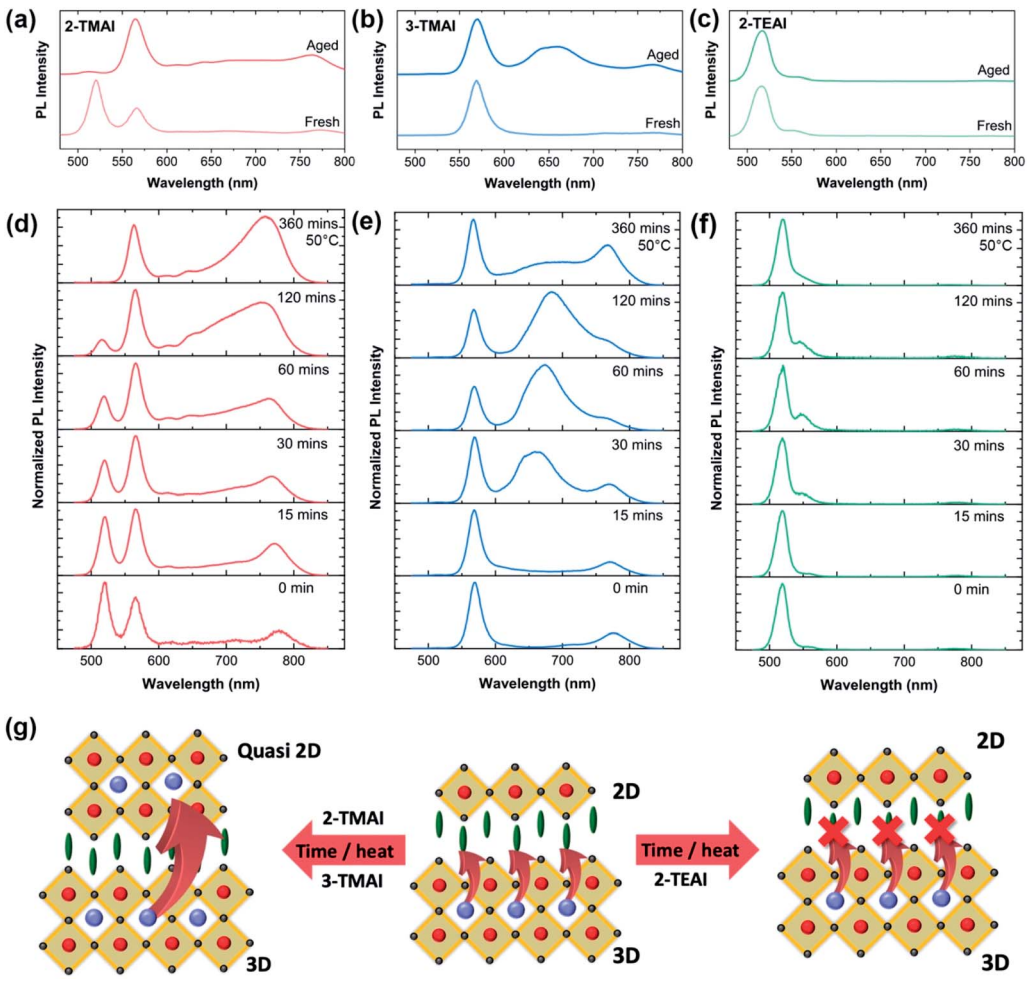

Fig. 3 PL spectra upon excitation at 450 nm of fresh and 4 months aged 2D/3D perovskite films employing (a) 2-TMAI, (b) 3-TMAI, and (c) 2-TEAI 2D/3D systems; PL spectra upon thermal stress (heating the film at 50 °C for the time as indicated in the legend) for (d) 2-TMAI, (e) 3-TMAI, and (f) 2-TEAI 2D/3D systems. (g) Cartoon illustrating the proposed interfacial mechanism.

of the 2D perovskite from a low n to a higher n quasi-2D/3D interface over time for all the cations (2-TMAI and 3-TMAI) except for the 2-TEAI based 2D/3D system.

To better elucidate the origin of this change, we simulate aging by stressing the thin films at 50 °C from 0 to 360 min and we measure the evolution of the PL spectra over time (Fig. 3d–f). A clear change in the emission peak position and relative intensity is again observed for the 2-TMAI and 3-TMAI 2D/3D films, while only a minor modification is observed for 2-TEAI films. More in detail, for 2-TMAI 2D/3D, the peak at 520 nm reduces in intensity in favor of the peak at 570 nm, vanishing completely after 360 min, while for 3-TMAI 2D/3D, the peak at 570 nm does not change. In both cases, a broad peak at a higher wavelength grows. In contrast, for 2-TEAI the 520 nm peak is mostly unaltered (a small shoulder at 550 nm appears) and no emission at longer wavelengths is observed. The broad red peak present in 2-TMAI and 3-TMAI can be related to the formation of the quasi-2D phase. This result matches with what is observed upon aging, pointing to a similar phenomenon behind such structural changes. It is worth mentioning that the aging does not degrade the 3D bulk underneath, since the absorption spectra of the films do not change (Fig. S15†) and also the XRD patterns of aged and thermally stressed films show no change in the 3D structures (Fig. S16 and S17†).

The preceding observations can be explained by the following mechanism as shown in Fig. 3g. The 2D perovskite, in the case of 2-TMAI and 3-TMAI, functions as a dynamical "sponge" that can embed small ions (such as MA or FA) migrating from the 3D bulk underneath immobilizing them into the new quasi-2D structure. This does not happen for the 2-TEAI 2D/3D that only physically blocks the ion at the interface, preserving the initial purity of the 2D phase ($n = 1$). We can thus infer that the presence of a structurally robust 2D layer (such as in the case of the 2-TEAI) is paramount to control device stability, demonstrating that the purity of the layered 2D structure and its robustness against ion movement and infiltration have a crucial impact on the long-term device stability. We can speculate that this is intimately related to the different packing motif of the organic cations dictated by the length of the side alkyl chain which imparts robustness to the 2D structure. Further work on the structural stability is the focus of ongoing work.

Conclusions

We revealed that 2D/3D interfaces are dynamical in nature, acting as ion-scavengers and self-transforming, upon aging or thermal stress, into quasi-2D graded interfaces. In general, the deposition of a 2D layer with various thiophene alkylammonium iodide cations protects the 3D layer from the degradation in the ambient air. This can improve the device performance upon dark aging, but does not lead to stable device operation under illumination. Proper engineering of the 2D/3D system, by judicious choice of the organic cation can lead to structurally stable and robust 2D overlayers (with $n = 1$) that have a decisive role in improving device stability under illumination. A careful molecular design of a large organic cation which can maintain the quasi-2D graded interface ($n = 2$) over dark aging and thermal stress is very important to deliver both stable and efficient PSCs. These observations pave the way for new avenues for the development of an intelligent molecular engineering approach to guide smart device design and application of stable 2D/3D interfaces even beyond PVs.

Conflicts of interest

There are no conflicts to declare.

Acknowledgements

This research used the 11-BM (CMS) beamline of the National Synchrotron Light Source II, a U.S. Department of Energy (DOE) Office of Science User Facility operated for the DOE Office of Science by Brookhaven National Laboratory under Contract No. DE-SC0012704. We acknowledge Dr Ruipeng Li for assistance at the beamline. We acknowledge Professor Raffaella Buonsanti for the use of the Fluorolog system and Dr Mounir Mensi for fruitful discussion. We acknowledge the Swiss National Science Foundation (SNSF) funding through the Ambizione Energy Project No. 646 HYPER (Grant No. PZENP2173641) and through the Synergia Grant EPISODE (Grant No. CRSII5_171000). G. G. acknowledges the "HY-NANO" project that has received funding from the European Research Council (ERC) Starting Grant 2018 under the European Union's Horizon 2020 research and innovation programme (Grant agreement No. 802862).

Notes and references

1 https://www.nrel.gov/pv/cell-efficiency.html.
2 E. H. Jung, N. J. Jeon, E. Y. Park, C. S. Moon, T. J. Shin, T.-Y. Yang, J. H. Noh and J. Seo, *Nature*, 2019, **567**, 511–515.
3 Q. Wang, Q. Dong, T. Li, A. Gruverman and J. Huang, *Adv. Mater.*, 2016, **28**, 6734–6739.
4 S. H. Turren-Cruz, A. Hagfeldt and M. Saliba, *Science*, 2018, **362**, 449–453.
5 M. Kim, S. G. Motti, R. Sorrentino and A. Petrozza, *Energy Environ. Sci.*, 2018, **11**, 2609–2619.
6 H. Peng, W. Sun, Y. Li, S. Ye, H. Rao, W. Yan, H. Zhou, Z. Bian and C. Huang, *Nano Res.*, 2016, **9**, 2960–2971.
7 N. Arora, M. I. Dar, A. Hinderhofer, N. Pellet, F. Schreiber, S. M. Zakeeruddin and M. Gratzel, *Science*, 2017, **358**, 768–771.
8 A. Agresti, S. Pescetelli, B. Taheri, A. E. Del Rio Castillo, L. Cina, F. Bonaccorso and A. Di Carlo, *ChemSusChem*, 2016, **9**, 2609–2619.
9 P. O'Keeffe, D. Catone, A. Paladini, F. Toschi, S. Turchini, L. Avaldi, F. Martelli, A. Agresti, S. Pescetelli, A. E. Del Rio Castillo, F. Bonaccorso and A. Di Carlo, *Nano Lett.*, 2019, **19**, 684–691.
10 L. Najafi, B. Taheri, B. Martín-García, S. Bellani, D. Di Girolamo, A. Agresti, R. Oropesa-Nuñez, S. Pescetelli, L. Vesce, E. Calabrò, M. Prato, A. E. Del Rio Castillo, A. Di Carlo and F. Bonaccorso, *ACS Nano*, 2018, **12**, 10736–10754.

11 D. H. Cao, C. C. Stoumpos, O. K. Farha, J. T. Hupp and M. G. Kanatzidis, *J. Am. Chem. Soc.*, 2015, **137**, 7843–7850.
12 C. C. Stoumpos, D. H. Cao, D. J. Clark, J. Young, J. M. Rondinelli, J. I. Jang, J. T. Hupp and M. G. Kanatzidis, *Chem. Mater.*, 2016, **28**, 2852–2867.
13 K. Yao, X. Wang, F. Li and L. Zhou, *Chem. Commun.*, 2015, **51**, 15430–15433.
14 C. Ma, C. Leng, Y. Ji, X. Wei, K. Sun, L. Tang, J. Yang, W. Luo, C. Li, Y. Deng, S. Feng, J. Shen, S. Lu, C. Du and H. Shi, *Nanoscale*, 2016, **8**, 18309–18314.
15 J. Chen, J.-Y. Seo and N.-G. Park, *Adv. Energy Mater.*, 2018, **8**, 1702714.
16 K. T. Cho, G. Grancini, Y. Lee, E. Oveisi, J. Ryu, O. Almora, M. Tschumi, P. A. Schouwink, G. Seo, S. Heo, J. Park, J. Jang, S. Paek, G. Garcia-Belmonte and M. K. Nazeeruddin, *Energy Environ. Sci.*, 2018, **11**, 952–959.
17 K. T. Cho, Y. Zhang, S. Orlandi, M. Cavazzini, I. Zimmermann, A. Lesch, N. Tabet, G. Pozzi, G. Grancini and M. K. Nazeeruddin, *Nano Lett.*, 2018, **18**, 5467–5474.
18 I. García-Benito, C. Quarti, V. I. E. Queloz, S. Orlandi, I. Zimmermann, M. Cavazzini, A. Lesch, S. Marras, D. Beljonne, G. Pozzi, M. K. Nazeeruddin and G. Grancini, *Chem. Mater.*, 2018, **30**, 8211–8220.
19 G. Grancini, C. Roldán-Carmona, I. Zimmermann, E. Mosconi, X. Lee, D. Martineau, S. Narbey, F. Oswald, F. De Angelis, M. Graetzel and M. K. Nazeeruddin, *Nat. Commun.*, 2017, **8**, 15684.
20 Y. Bai, S. Xiao, C. Hu, T. Zhang, X. Meng, H. Lin, Y. Yang and S. Yang, *Adv. Energy Mater.*, 2017, **7**, 1701038.
21 T. M. Koh, V. Shanmugam, X. Guo, S. S. Lim, O. Filonik, E. M. Herzig, P. Müller-Buschbaum, V. Swamy, S. T. Chien, S. G. Mhaisalkar and N. Mathews, *J. Mater. Chem. A*, 2018, **6**, 2122–2128.
22 G. Grancini and M. K. Nazeeruddin, *Nat. Rev. Mater.*, 2019, **4**, 4–22.
23 C. Ortiz-Cervantes, P. Carmona-Monroy and D. Solis-Ibarra, *ChemSusChem*, 2019, **12**, 1560–1575.
24 B. Roose, A. Ummadisingu, J.-P. Correa-Baena, M. Saliba, A. Hagfeldt, M. Graetzel, U. Steiner and A. Abate, *Nano Energy*, 2017, **39**, 24–29.
25 J. M. Azpiroz, E. Mosconi, J. Bisquert and F. De Angelis, *Energy Environ. Sci.*, 2015, **8**, 2118–2127.
26 D. Meggiolaro, E. Mosconi and F. De Angelis, *ACS Energy Lett.*, 2019, **4**, 779–785.
27 Y. Yuan and J. Huang, *Acc. Chem. Res.*, 2016, **49**, 286–293.
28 M. E. F. Bouduban, V. I. E. Queloz, V. M. Caselli, K. T. Cho, A. R. Kirmani, S. Paek, C. Roldan-Carmona, L. J. Richter, J. E. Moser, T. J. Savenije, M. K. Nazeeruddin and G. Grancini, *J. Phys. Chem. Lett.*, 2019, **10**, 5713–5720.
29 S. R. Cowan, A. Roy and A. J. Heeger, *Phys. Rev. B: Condens. Matter Mater. Phys.*, 2010, **82**, 245207.
30 Z. Liu, S. Niu and N. Wang, *J. Colloid Interface Sci.*, 2018, **509**, 171–177.
31 K. Domanski, J.-P. Correa-Baena, N. Mine, M. K. Nazeeruddin, A. Abate, M. Saliba, W. Tress, A. Hagfeldt and M. Grätzel, *ACS Nano*, 2016, **10**, 6306–6314.

